Applied Physics A (2020) 126:495
https://doi.org/10.1007/s00339-020-03687-z

Applied Physics A
Materials Science & Processing

Effect of molybdenum doping on the structural and magnetic properties of $MnFe_2O_4$ magnetic nanoparticles

F. Al-Mokdad[1] · Z. Bitar[1] · R. Sayed Hassan[2] · N. Yaacoub[3] · R. Awad[1]

Received: 31 March 2020 / Accepted: 30 May 2020 / Published online: 8 June 2020

Abstract
Magnetic nanoparticles $MnFe_{2-x}Mo_xO_4$ ($x=0.00$, 0.04, 0.08 and 0.10) have been prepared by wet coprecipitation method at calcination temperature 673 K. *X*-ray powder diffraction (XRD) was used to study the structural properties of the prepared samples, whereas the vibrating sample magnetometer (VSM) and Mössbauer spectrometry measurements (at $T=300$ K and $T=77$ K) were used to investigate the magnetic properties. The single-phase cubic spinel structure of the ferrites samples was confirmed by the XRD patterns, and a nonlinear variation in the crystalline size was revealed. VSM hysteresis loops confirmed the ferromagnetic behavior in all the samples with an increase in saturation magnetization with the molybdenum doping. Mössbauer spectra at 300 K showed a mixture of the magnetic sextet and central quadrupole doublet with enhancement in the magnetic sextet in the Mo-doped samples. Moreover, Mössbauer spectra at 77 K revealed the disappearance of the quadrupole doublet in all samples, indicating the enhancement of magnetic properties of manganese ferrites nanoparticles due to Mo-doping.

Keywords Mo-doped ferrites · Magnetic nanoparticles · Magnetic properties · Mössbauer spectrometry

1 Introduction

Among the various types of nanomaterials that found very wide practical applications in technology, ferrites caught great attention. Ferrites nanoparticles, by their fascinating properties, are the most explored magnetic nanoparticles up to date. The high saturation magnetization (M_s), high electric resistivity, low dielectric loss and the very good chemical stability [1–4] are all properties that make ferrites nanoparticles important candidate in many applications as in inductors, high-frequency systems as well as other biotechnological applications.

The properties of spinel ferrites nanoparticles depend on many various factors and mainly on the cations distributions among the tetrahedral and octahedral sites. Therefore, they are sensitive to the presence of doping cations, the types and the amounts of these cations. Many researchers have focused on investigating the effect of doping on spinel ferrites nanoparticles with various types of dopants [5–7]. Among different types of dopants, transition metal (TM) ions have shown significant effects and changes in the structural, optical, electric, and magnetic properties of spinel ferrites nanoparticles [8–10]. Various TM ions such as Mn, Cu, Ni, Cd, Co, and Mo were used as dopants on several kinds of spinel nanoferrites, and their consequent effects on the different physical properties of these nanoferrites were reported [11–15]. Kumar et al. [15] reported that Mn-doping on $CoFe_2O_4$, $NiFe_2O_4$, $CuFe_2O_4$, and $ZnFe_2O_4$ nanoparticles, makes them good sensors for the LPG (liquefied petroleum gas) with higher responses for the Mn-Zn ferrites nanoparticles. Velinov et al. [16] found that Cu-doped manganese ferrites nanoparticles reveal higher catalytic activity than the pure $CuFe_2O_4$ and $MnFe_2O_4$ nanoferrites in the methanol decomposition. Moreover, the optical limiting studies performed by Yuvaraj et al. [17] show that the Cu-doped manganese ferrites nanoparticles are potential candidates for optoelectronic device fabrication. Also, magnetic properties of $ZnFe_2O_4$ and $CrNiFe_2O_4$ nanoparticles were enhanced when doped by Ni and Co transition metals, respectively [18, 19].

✉ Z. Bitar
zouheirbitar@hotmail.com

[1] Department of Physics, Faculty of Science, Materials Science Lab, Beirut Arab University, Beirut, Lebanon

[2] Department of Physics, Faculty of Science, Lebanese University, Beirut, Lebanon

[3] Institut Des Molécules Et Matériaux du Mans (IMMM) CNRS UMR-6283, Le Mans Université, Avenue Messiaen, 72085 Le Mans, France

On the other hand, Mo-doping was carried out on cobalt and zinc ferrites. It was reported that Mo substituted successfully the single-phase cubic structure of spinel ferrites and affected greatly the magnetic properties of both Co and Zn ferrites [20, 21].

In the current work, manganese ferrites nanoparticles ($MnFe_2O_4$) doped by molybdenum were prepared by the wet coprecipitation method. To investigate their structural properties, XRD technique was used. Moreover, magnetic measurement, as well as Mössbauer studies, was carried out to study the effect of molybdenum on their physical parameters such as saturation magnetization, coercivity, and hyperfine parameters (isomer shift, quadrupole shifts, hyperfine field).

2 Experimental methods

Manganese ferrites nanoparticles with the formula $MnFe_{2-x}Mo_xO_4$ ($x = 0.00$, 0.04, 0.08, and 0.10) were prepared by using the wet chemical coprecipitation method. In this method, metal chlorides such as ferric chloride ($FeCl_3{\cdot}6H_2O$), manganese chloride ($MnCl_2{\cdot}4H_2O$), and molybdenum chloride ($MoCl_5$) were mixed in distilled water as starting materials. Raising the pH to 12.5 was carried out by adding sodium hydroxide solution (NaOH). Then, washing with distilled water was done until pH becomes 7. The samples were then dried at temperature of 353 K for 24 h. Finally, the powder samples of $MnFe_{2-x}Mo_xO_4$ were heated for 4 h at a calcination temperature of 673 K.

$MnFe_{2-x}Mo_xO_4$ samples were characterized by using PANalytical X'Pert Pro diffractometer (Co-Kα radiation with $\lambda = 1.78901$ Å), Vibrating Sample Magnetometer (Lake Shore 7410), and ^{57}Fe Mössbauer spectrometry measurements were taken at both temperatures $T = 300$ K and $T = 77$ K, by using a ^{57}Co/Rh γ-ray source mounted on an electromagnetic drive, using a triangular velocity form, in a transmission scheme.

The lattice parameters and the size of the coherent diffraction domain were determined with MAUD software [22], which is based on the Rietveld method combined with Fourier analysis. For Mössbauer data analysis, the 'MOSFIT' program was used (unpublished program). The hyperfine structures were modeled by involving Zeeman sextets and quadrupole doublets composed of Lorentzian lines. The isomer shift (δ) values were referred to that of α-Fe at 300 K.

3 Results and discussion

3.1 Structural analysis

The XRD patterns of $MnFe_{2-x}Mo_xO_4$ ($x = 0.00$, 0.04, 0.08, and 0.1) samples are shown in Fig. 1. The main diffraction peaks are corresponding to (220), (311), (400), (511), and (440) planes. All the detected peaks confirmed the formation of the single-phase spinel structure of $MnFe_2O_4$ with space group Fd-3 m (JCPDS card no.75-0034). Similar results were reported by Ansari and Khan for Co-doped $MnFe_2O_4$ prepared by using the sol–gel technique [23]. Ansari and Khan reported the formation of the single-phase cubic spinel structure of the Co–$MnFe_2O_4$ samples with no unreacted constituents or impurity phases. The lattice parameters and crystalline size of $MnFe_{2-x}Mo_xO_4$ ($x = 0.00$, 0.04, 0.08, and 0.1) samples are listed in Table 1.

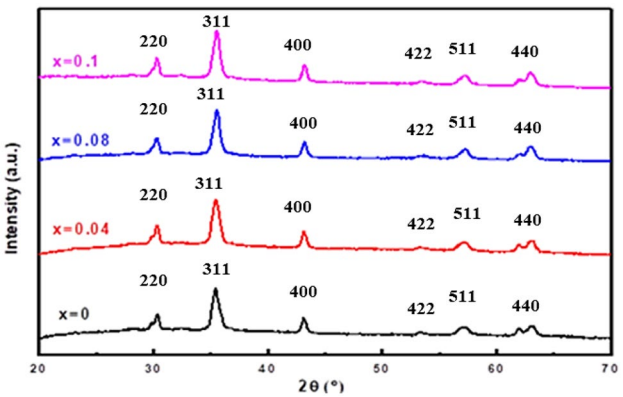

Fig.1 XRD patterns of $MnFe_{2-x}Mo_xO_4$ ($0 \le x \le 0.1$) nanoparticles

Table 1 The variation of lattice parameters and crystalline size of $MnFe_{2-x}Mo_xO_4$ ($0 \le x \le 0.1$) nanoparticles

Samples	Lattice parameter a (Å)	Crystalline size (nm)
$MnFe_2O_4$	8.391	22
$MnFe_{1.96}Mo_{0.04}O_4$	8.385	19
$MnFe_{1.92}Mo_{0.08}O_4$	8.375	23
$MnFe_{1.9}Mo_{0.1}O_4$	8.353	31

The average crystalline size was determined by XRD Rietveld refinement using MAUD [24]. As Table 1 shows, the crystalline size of the samples indicates a nonlinear variation with Mo-doping. The crystalline size first decreases for low Mo-doping from 22 nm for pure manganese ferrite sample ($x = 0$) to 19 nm for the sample with $x = 0.04$, whereas a further increase in Mo-doping leads to the increase in the crystalline size to reach 31 nm for the sample with $x = 0.1$. Similar kinds of findings were reported by Joshi et al. [25] for Ni-doped cobalt ferrites where the crystalline size decreased with $x = 0.5$ and then increased for $x = 1$, whereas the difference in tetrahedral and octahedral ionic radii of both Fe^{3+} and Mo^{5+} ions can be considered the reason behind the reduction in the lattice parameter with the increase in Mo-doping. The tetrahedral ionic radius of Fe^{3+} ions (0.49 Å) is greater than the tetrahedral ionic radius

of Mo^{5+} ions (0.46 Å), and the octahedral ionic radius of Fe^{3+} ions (0.55 Å) is greater than the octahedral ionic radius of Mo^{5+} ions (0.61 Å). Heiba et al. [20] reported a similar decrease in lattice parameter $CoFe_2O_4$ nanoparticles doped by molybdenum and prepared by the solution combustion method.

3.2 Magnetic properties

Figure 2 displays the magnetic hysteresis (M-H) curves of $MnFe_{2-x}Mo_xO_4$ showing that all the samples exhibit a long range of ferromagnetic ordering. For all samples, the hysteresis loops open at low fields (see inset of Fig. 2) and approach the saturation magnetization at about 10 kg. The magnetic properties of ferrites usually depend on morphology, crystalline size and mainly the superexchange couplings between the magnetic cations via the mediating oxygen O^{2-}anions [7]. Figure 3 shows the variation in saturation magnetization M_s as a function of Mo content. The value of M_s increased with Mo content from 22.8 emu/g for the pure manganese ferrite ($x=0$) to 39.0 emu/g for $MnFe_{1.96}Mo_{0.04}O_4$ sample ($x=0.04$) and then decreases as Mo increased to reach 33.1 emu/g for $MnFe_{1.9}Mo_{0.1}O_4$ sample ($x=0.1$).

The magnetic order of the ferromagnetic in the spinel cubic system is mainly due to the superexchange interactions occurring between the metal cations in tetrahedral (A) and octahedral (B) sites. Therefore, the variation of saturation magnetization of $MnFe_{2-x}Mo_xO_4$ samples is related to the cations distribution among A and B sites. Based on Neel's molecular field model [26], the (A-B) interactions are much stronger than (A–A) and (B–B) interactions. For spinel ferrites, the net magnetic moment of the lattice is obtained by the vector sum of magnetic sublattices A and B: $M(x)=M_B(x)-M_A(x)$, where M_B and M_A represent the magnetic moment of octahedral and tetrahedral sites, respectively. Therefore, the enhancement of saturation magnetization attained at low Mo-doping by sample with ($x=0.04$) may be attributed to the replacement of Fe^{3+} ions in the tetrahedral sites by Mo^{5+} ions. At this low doping of Mo, the occupancy of Fe^{3+} ions in the octahedral sites is not affected. However, the entrance of one Mo^{5+} ion into the manganese ferrite structure forces two Fe^{3+} ions to expel from the A sites causing the increase in M_s. Dwivdedi et al. [27] reported that the occupancy of Mo ions in the tetrahedral sites of cobalt ferrites caused the increase in M_s values with increased doping, whereas the decrease in M_s for higher Mo-doping of the $MnFe_{2-x}Mo_xO_4$ samples with $x \geq 0.08$ may be attributed to the accommodation of some Mo^{5+} ions in octahedral sites leading to the reduction in the moment of B site and

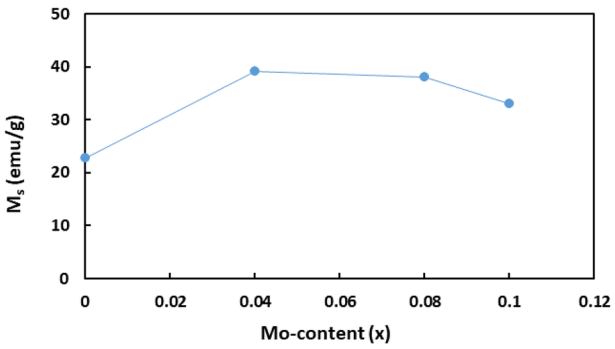

Fig.3 The variation of saturation magnetization M_s (emu/g) of $MnFe_{2-x}Mo_xO_4$ nanoparticles as a function of the Mo content (x)

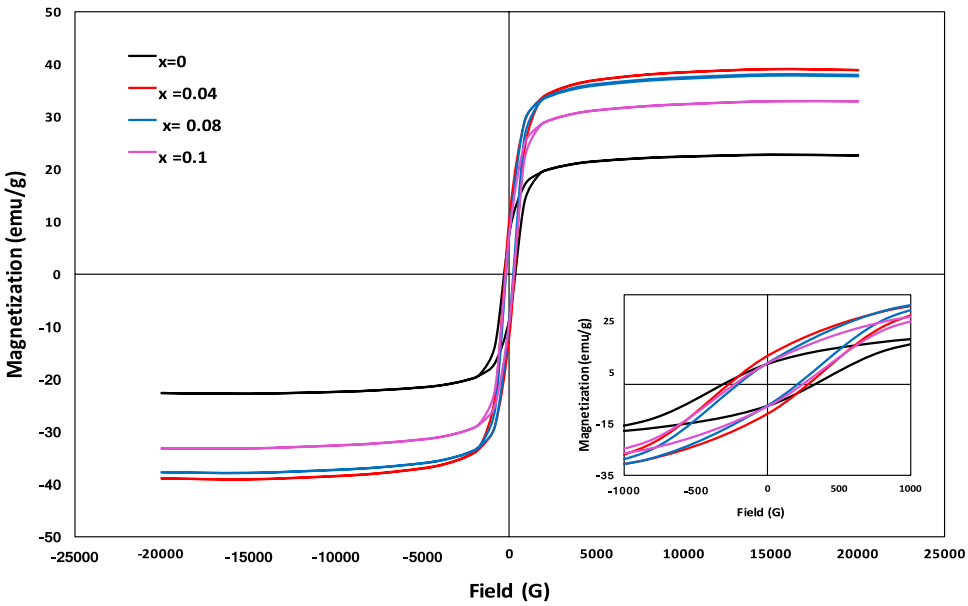

Fig.2 M–H loops for $MnFe_{2-x}Mo_xO_4$ with ($0 \leq x \leq 0.1$) at room temperature

hence the saturation magnetization. Similar behavior of M_s variation was reported by Heiba et al. [20] for Mo-doped $CoFe_2O_4$ in which the M_s values increased up to $x = 0.15$ and then decreased for $x \geq 0.2$.

On the other hand, the variation of the coercivity (H_c) values of $MnFe_{2-x}Mo_xO_4$ samples and the crystalline size (D) with the Mo content (x) is shown in Fig. 4. The coercivity value is observed to attain an overall decrease with the increase of crystalline size and Mo content. Spinel ferrites usually form crystallites that act as a single domain in deciding the magnetization nature of the material. However, when the crystalline size increases, the crystallite breaks up to form a number of small domains to reduce the large magnetization energy. This consequently causes a decrease in coercivity due to the contribution of domain walls [28]. The remanence ratio of all the prepared samples is less than 0.5 which means that they are multidomain nanoparticles [29]. In the case of the multidomain region, the coercivity decreases as the particle size increases according to the following relation:

$$H_c = a + \frac{b}{D}, \tag{1}$$

where a and b are constants, and D is the particle size [30]. A similar decrease in H_c with the increase in crystalline size was observed in Co–Zn ferrites nanoparticles [31].

3.3 Mössbauer spectroscopy

In order to get more information about the effect of molybdenum of the structural and magnetic properties of manganese ferrite nanoparticles, ^{57}Fe Mössbauer spectra of $MnFe_{2-x}Mo_xO_4$ samples were recorded at room temperature $T = 300$ K and at low temperature $T = 77$ K without applying any external field.

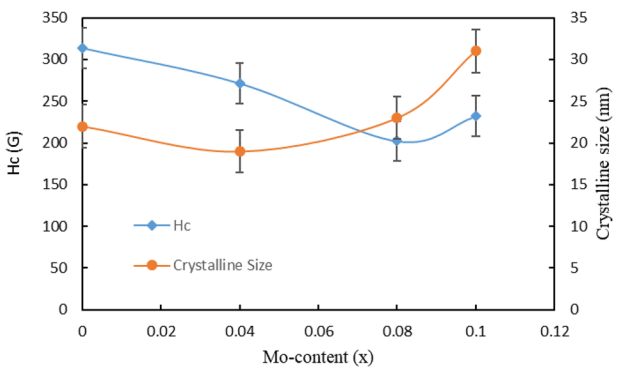

Fig.4 The variation of coercivity H_c (G) and crystalline size D (nm) of $MnFe_{2-x}Mo_xO_4$ nanoparticles as function of the Mo content (x)

3.3.1 Room temperature Mössbauer spectrometry

Figure 5 represents the spectra at room temperature of $MnFe_{2-x}Mo_xO_4$ samples with $x = 0$, 0.04, 0.08, and 0.1. The Mössbauer spectra show a mixture of a magnetic state characterized by a six-line pattern (sextet) corresponding to Fe cations occupying tetrahedral (A) and octahedral (B) sites in the unit cell, and a partial paramagnetic state (central quadrupole doublet). The mean values for all samples of the various Mössbauer parameters like isomer shift (δ), quadrupole splitting (Δ), hyperfine field (B_{hyp}), and the relative percent (%) are presented in Table 2. The obtained values of isomer shift $<\delta>$ in all samples are typical of the Fe^{3+} ions, and we could exclude the presence of Fe^{2+} ions [32].

It is shown that as Mo-doping increases, the percentage of the magnetic contribution increases, whereas the doublet decreases from 36% for pure sample ($x = 0$) to 18% for the sample with maximum Mo-doping ($x = 0.1$). The presence of the quadrupolar doublet, that is superimposed on magnetically split sextets, may be due to the distribution in the grain size and the presence of superparamagnetic behavior in

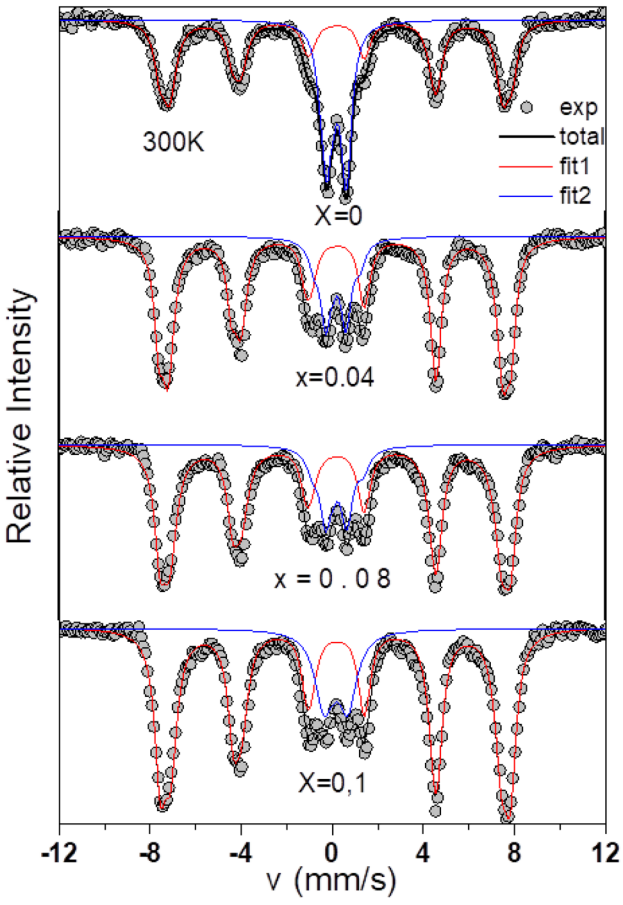

Fig.5 Mössbauer spectra of the $MnFe_{2-x}Mo_xO_4$ nanoparticles at $T = 300$ K

Table 2 Different hyperfine parameters obtained from fitting the Mössbauer spectra of $MnFe_{2-x}Mo_xO_4$ nanoparticles with $x=0$, 0.04, 0.08, and 0.1 at $T=300$ K

Sample	$T=300$ K	$<\delta>$ (mm/s)	$<\Delta>$ (mm/s)	$<B_{hyp}>(T)$	Relative area %
$x=0$	Doublet	0.33	0.828	0	36
	Sextet	0.34	−0.026	46.0	64
$x=0.04$	Doublet	0.31	0.973	0	20
	Sextet	0.33	−0.062	46.2	80
$x=0.08$	Doublet	0.32	0.6	0	18
	Sextet	0.33	−0.04	46	82
$x=0.1$	Doublet	0.28	0.949	0	18
	Sextet	0.33	−0.04	46.1	82

addition to ferromagnetic one [33]. However, the increase in the magnetic contribution with Mo-doping may be attributed to the variation of the crystalline size which was revealed by the XRD analysis where the size was decreased for $x=0.04$ and then increased for $x>0.04$. Therefore, the crystallite size should be taken into consideration in addition to the effect of Mo-doping on the manganese ferrite. When the particle size decreases, the surface to volume ratio became more significant which can be attributed to the increase of the spin disorder on the surface of nanoparticles. The surface spin disorder is due to the modification of the exchange interactions between surface magnetic ions in incomplete coordination. Therefore, the surface to volume ratio affects the magnetic properties. When the particle size increases, the effective anisotropy constant decreases. The magnetic states of the core and the surface of the nanoparticles are different. Therefore, the increase of magnetization can be attributed to the independence of the core magnetic moment and the surface moments where coupling reaches a finite state of superexchange interaction [34, 35]. Similar behavior was observed by Srinivas et al. [33] in Ni–Zn ferrites where they reported the increase in the intensity of sextets due to an increase in crystalline size. Siddique and Butt [36] reported the presence of paramagnetic quadrupole doublet in $MnFe_2O_4$ nanoparticles prepared by the coprecipitation method in addition to the magnetic sextet, and its relative contribution was found to be 58% attributing it to the superparamagnetic relaxation effect.

3.3.2 $T=77$ K Mössbauer spectrometry

To investigate the thermal effect, the Mössbauer measurement was taken at 77 K for all samples. As illustrated in Fig. 6 the hyperfine structure consists mainly of magnetic sextets. The spectrum for $x=0$ is fitted by a sextet, and a discrete distribution of hyperfine fields correlated with

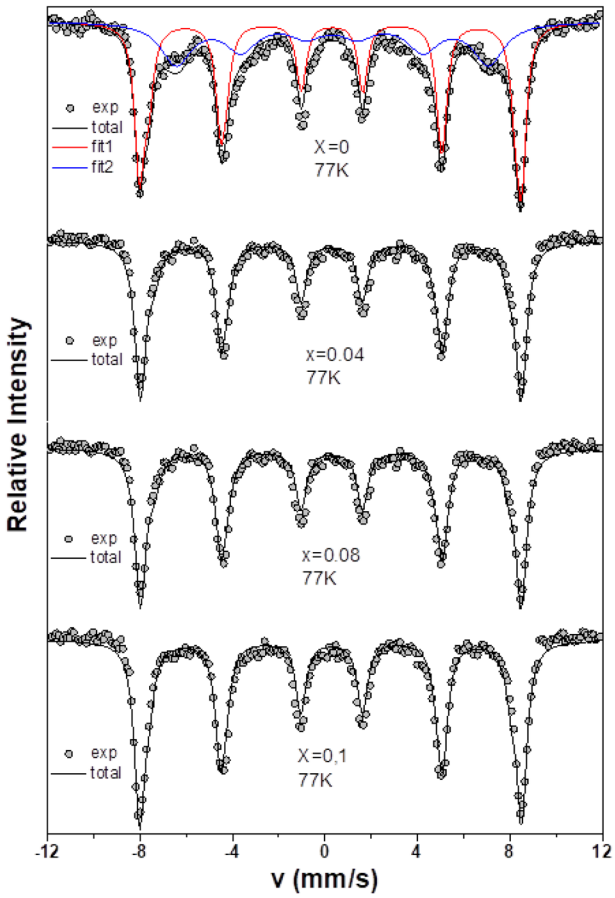

Fig.6 Mössbauer spectra of the $MnFe_{2-x}Mo_xO_4$ nanoparticles at $T=77$ K

that of isomer shift to describe the asymmetrical profile of lines. All samples consist of broadened six-line and asymmetrical patterns without any observed quadrupole doublet. The disappearance of the quadrupole doublets in both samples at $T=77$ K, confirms that those obtained at room temperature were due to thermal superparamagnetic fluctuations.

The mean values of the different Mössbauer parameters for all samples are shown in Table 3. According to this table, the magnetic contribution due to the distribution in the grain size still exists only in the pure sample ($x=0$) with percentage equals to 40%; however, with the Mo-doping the percentage of magnetic contribution due to the occupancy of Fe^{3+} ions on A/B sites increased to become 100% in all Mo-doped samples. This is in agreement with the room temperature results, which confirmed the increase in magnetic contribution due to crystalline size increase. The mean isomer values obtained (in the range 0.43 and 0.45 mm/s) indicate the presence of only Fe^{3+} ions, in agreement with room temperature results.

Table 3 Mean hyperfine parameters obtained from fitting the Mössbauer spectra of $MnFe_{2-x}Mo_xO_4$ samples with $x=0$, 0.04, 0.08, and 0.1 at $T=77$ K

Sample	$T=77$ K	$<\delta>$ (mm/s)	$<\Delta>$ (mm/s)	$<B_{hyp}>$ (T)	Relative area %
$x=0$	Sextets Fe^{3+}(A/B)	0.45	−0.05	50.8	60
	Sextets distribution	0.47	0.02	41.7	40
$x=0.04$	Sextets Fe^{3+}(A/B)	0.44	−0.04	50.5	100
	Sextets distribution	–	–	–	–
$x=0.08$	Sextets Fe^{3+}(A/B)	0.44	−0.038	50.3	100
	Sextets distribution	–	–	–	–
$x=0.1$	Sextets Fe^{3+}(A/B)	0.43	−0.05	50.5	100
	Sextets distribution	–	–	–	–

4 Conclusion

$MnFe_{2-x}Mo_xO_4$ nanoparticles were successfully prepared by the wet coprecipitation method. The XRD analysis revealed that all samples obtain a single-phase cubic spinel structure and a nonlinear variation in the crystalline size. The room temperature (M–H) loops of $MnFe_{2-x}Mo_xO_4$ samples showed the ferromagnetic behavior in all samples with an increase in the values of Ms with Mo-doping, while those of *Hc* decreased. Mössbauer spectrometry measurements at $T=300$ K revealed the presence of a mixture of the magnetic sextet and central quadrupole doublet in all samples. However, an enhancement in the relative area of the magnetic sextet and decrease in that for the doublet appeared in the Mo-doped samples. On the other hand, Mössbauer spectra at 77 K revealed the disappearance of the quadrupole doublet in all samples, indicating the enhancement of magnetic properties of manganese ferrites nanoparticles due to Mo-doping.

Acknowledgement This work was achieved in the materials science laboratory, Physics department, Faculty of Science, Beirut Arab University, Beirut, Lebanon, in collaboration with the Physics department, Faculty of Science, Lebanese University. The authors are thankful for the Institute des Molecules et Matériaux du Mans (IMMM), Le Mans, France for the Mössbauer data collection, and the Faculty of Science, Alexandria University, Alexandria, Egypt.

References

1. R. Valenzuela, Phys. Res. Int. **2012**, 1 (2012)
2. D. Peddis, N. Yaacoub, M. Ferretti, A. Martinelli, G. Piccaluga, A. Musinu, C. Cannas, G. Navarra, J.M. Greneche, D. Fiorani, J. Phys. Condens. Matter **23**, 426004 (2011)
3. M. Artus, L.B. Tahar, F. Herbst, L. Smiri, F. Villain, N. Yaacoub, J.-M. Grenèche, S. Ammar, F. Fiévet, J Phys Condens Matter **23**, 506001 (2011)
4. G. Muscas, N. Yaacoub, G. Concas, F. Sayed, R.S. Hassan, J.M. Greneche, C. Cannas, A. Musinu, V. Foglietti, S. Casciardi, C. Sangregorio, D. Peddis, Nanoscale **7**, 13576 (2015)
5. D.S. Mathew, R.-S. Juang, Chem. Eng. J. **129**, 51 (2007)
6. A.M. Wahba, M.B. Mohamed, Ceram Int **40**, 6127 (2014)
7. R.A. Pawar, S.S. Desai, S.M. Patange, S.S. Jadhav, K.M. Jadhav, Phys B: Condens. Matter **510**, 74 (2017)
8. D. Ravinder, A.V.R. Reddy, G.R. Mohan, Mater Lett **52**, 259 (2002)
9. K.M. Batoo, S. Kumar, C.G. Lee, and Alimuddin. Curr. Appl. Phys. **9**, 1397 (2009)
10. O. Mounkachi, M. Hamedoun, M. Belaiche, A. Benyoussef, R. Masrour, H. El Moussaoui, M. Sajieddine, Phys B: Condens. Matter **407**, 27 (2012)
11. C.V. Ramana, Y.D. Kolekar, K. Kamala Bharathi, B. Sinha, K. Ghosh, J Appl Phys **114**, 183907 (2013)
12. M. Khaleghi, H. Moradmard, S.F. Shayesteh, IEEE T. Magn. **54**, 1 (2018)
13. N.B. Velhal, N.D. Patil, A.R. Shelke, N.G. Deshpande, V.R. Puri, AIP Adv. **5**, 097166 (2015)
14. K. Kombaiah, J.J. Vijaya, L.J. Kennedy, M. Bououdina, K. Kaviyarasu, R.J. Ramalingam, M.A. Munusamy, A. AlArfaj, Optik **135**, 190 (2017)
15. E.R. Kumar, P.S.P. Reddy, G.S. Devi, S. Sathiyaraj, J Magn Magn Mater **398**, 281 (2016)
16. N. Velinov, T. Petrova, I. Genova, I. Ivanov, T. Tsoncheva, V. Idakiev, B. Kunev, I. Mitov, Mater. Res. Bull. **95**, 556 (2017)
17. S. Yuvaraj, N. Manikandan, G. Vinitha, Opt. Mater. **73**, 428 (2017)
18. S.S. Kumbhar, M.A. Mahadik, V.S. Mohite, K.Y. Rajpure, J.H. Kim, A.V. Moholkar, C.H. Bhosale, J. Magn. Magn. Mater. **363**, 114 (2014)
19. S. Singhal, S. Bhukal, J. Singh, K. Chandra, S. Bansal, J. Nanotechnol. **2011**, 1 (2011)
20. Z.K. Heiba, N.Y. Mostafa, O.H. Abd-Elkader, J. Magn. Magn. Mater. **368**, 246 (2014)
21. Z.K. Heiba, M.B. Mohamed, A.M. Wahba, J. Mol. Struct. **1108**, 347 (2016)
22. L. Lutterotti, S. Matthies, and H. R. Wenk, International Union of Crystallography. Newsletter No. 21, May 1999. pp. 14–15. http://www.iucr.org/iucr-top/comm/cpd/Newsletters/ (1999)
23. M.M.N. Ansari, S. Khan, Phys. B Condens. Matter **520**, 21 (2017)
24. L. Lutterotti, M. Bortolotti, G. Ischia, I. Lonardelli and H. R. Wenk, Rietveld texture analysis from diffraction images. (Z. Kristallogr. Suppl. 26, 2007) pp. 125–130
25. G.P. Joshi, N.S. Saxena, R. Mangal, A. Mishra, T.P. Sharma, Bull. Mater. Sci. **26**, 387 (2003)
26. M. Atif, S.K. Hasanain, M. Nadeem, Solid State Commun. **138**, 416 (2006)
27. G.D. Dwivedi, K.F. Tseng, C.L. Chan, P. Shahi, J. Lourembam, B. Chatterjee, A.K. Ghosh, H.D. Yang, S. Chatterjee, Phys. Rev. B **82**, 134428 (2010)
28. S. Singhal, S. Jauhar, K. Chandra, S. Bansal, Bull. Mater. Sci. **36**, 107 (2013)
29. S. Satpute, S. Wadgane, K. Desai, D. Mane, R. Kadam, Ceramica **66**, 43 (2020)
30. M. Zhang, Z. Zi, Q. Liu, P. Zhang, X. Tang, J. Yang, X. Zhu, Y. Sun, J. Dai, Adv. Mater. Sci. Eng. **2013**, 609819 (2013)

31. M. Ben Ali, K. El Maalam, H. El Moussaoui, O. Mounkachi, M. Hamedoun, R. Masrour, E.K. Hlil, A. Benyoussef, J Magn Magn Mater **398**, 20 (2016)
32. M. Sorescu, L. Diamandescu, R. Peelamedu, R. Roy, P. Yadoji, J. Magn. Magn. Mater. **279**, 195 (2004)
33. Ch Srinivas, B.V. Tirupanyam, S.S. Meena, S.M. Yusuf, ChS Babu, K.S. Ramakrishna, D.M. Potukuchi, D.L. Sastry, J. Magn. Magn. Mater. **407**, 135 (2016)
34. R. Kamble, V. Varade, K. Ramesh, V. Prasad, AIP Adv. **5**, 017119 (2015)
35. B. Issa, I. Obaidat, B. Albiss, Y. Haik, Int. J. Mol. Sci. **14**, 21266–21305 (2013)
36. M. Siddique, N.M. Butt, Phys. B Condens. Matter **405**, 4211 (2010)